Research Article | Vol. 30, No. 7 / 28 Mar 2022 / Optics Express 11036
Optics EXPRESS

Optical fiber thermo-refractometer

J. J. IMAS,[1,2,*] C. R. ZAMARREÑO,[1,2] I. DEL VILLAR,[1,2] J. C. C. DA SILVA,[3] V. OLIVEIRA,[3] AND I. R. MATÍAS[1,2]

[1]*Electrical, Electronic and Communications Engineering Department, Public University of Navarra, 31006 Pamplona, Spain*
[2]*Institute of Smart Cities (ISC), Public University of Navarra, 31006 Pamplona, Spain*
[3]*Federal University of Technology - Parana (UTFPR), Curitiba 80230-901, Brazil*
[*]*josejavier.imas@unavarra.es*

Abstract: This work presents the implementation of a thermo-refractometer, which integrates the measurement of both refractive index and temperature in a single optical fiber structure. To this purpose, a lossy mode resonance (LMR)-based refractometer is obtained by means of the deposition of a titanium dioxide (TiO_2) thin film onto a side-polished (D-shaped) single mode fiber. Measurement and subsequent temperature compensation are achieved by means of a fiber Bragg grating (FBG) inscribed in the core of the D-shaped region. The LMR wavelength shift is monitored in transmission while the FBG (FBG peak at 1533 nm) displacement is observed in reflection. The LMR is sensitive to both the surrounding refractive index (SRI), with a sensitivity of 3725.2 nm/RIU in the 1.3324–1.3479 range, and the temperature (- 0.186 nm/°C); while the FBG is only affected by the temperature (32.6 pm/°C in the 25°C – 45°C range). With these values, it is possible to recover the SRI and temperature variations from the wavelength shifts of the LMR and the FBG, constituting a thermo-refractometer, where it is suppressed the effect of the temperature over the refractometer operation, which could cause errors in the fourth or even third decimal of the measured SRI value.

1. Introduction

The measurement of the refractive index of a medium depends on several parameters, being temperature one of the most important [1]. Therefore, to make a precise measurement of the refractive index at a given wavelength, it is necessary to know the temperature at which the measurement is made. In fact, in biomedical applications, temperature sensing is relevant [2] and being able to measure the refractive index and the temperature simultaneously using the same sensor head is very convenient. In this sense, this work presents a sensor head that incorporates a lossy mode resonance (LMR) based refractometer and an FBG based temperature sensor. Both of them are implemented in a single D-shaped fiber.

Lossy Mode Resonances (LMRs) are based on light coupling due to the deposition of a thin-film on a dielectric medium. They take place when the real part of the thin-film permittivity is positive and greater in absolute value than its own imaginary part and the real part of the permittivity of the waveguide, so metallic oxides and polymers can be employed to generate these resonances [3]. In addition to this, LMRs can be obtained with both transverse electric (TE) and transverse magnetic (TM) polarization [4]. One common application of LMRs is the development of refractometers [5–9].

Fiber Bragg gratings (FBGs) consist of periodic perturbations of the refractive index along a fiber (usually, a single mode fiber) formed by exposure of the core to an intense optical interference pattern [5,10]. Among them, short-period fiber Bragg gratings, generally denominated fiber Bragg gratings (FBGs), are the ones in which light coupling takes place between the core mode and counter-propagating modes. In standard FBGs there is a coupling with the counter-propagating core mode, whereas in tilted fiber Bragg gratings (TFBGs) there is a coupling with

#450316 https://doi.org/10.1364/OE.450316
Journal © 2022 Received 9 Dec 2021; revised 25 Jan 2022; accepted 8 Feb 2022; published 17 Mar 2022

Optics EXPRESS

counter-propagating cladding modes. That is the reason why FBGs, contrary to TFBGS, are not sensitive to the surrounding refractive index (SRI) variation, since light coupling occurs between core modes and the core is separated from the external medium by the fiber cladding [5]. However, FBGs are sensitive to temperature and strain as these variables affect both n_{core} and Λ [11], and therefore the Bragg wavelength [5], as stated in Eq. (1):

$$\lambda_{FBG} = 2 \cdot n_{eff\ core}(\lambda_{FBG}) \cdot \Lambda \tag{1}$$

where λ_{FBG} is the Bragg wavelength, $n_{eff\ core}(\lambda_{FBG})$ is the effective refractive index of the core mode at λ_{FBG} and Λ is the grating pitch.

Hence, one application of FBGs is temperature compensation in different types of sensors. In these cases, the magnitude of interest is measured with the sensor, but it does not affect the Bragg wavelength of the FBG. The temperature affects both the sensor and the Bragg wavelength. This way, the temperature variation can be extracted from the wavelength shift of the FBG and be compensated in the sensor to recover the value of the parameter of interest.

For instance, in [12] the interference fringe of a no-core fiber (NCF) is employed to measure the liquid level. This fringe is also sensitive to the temperature. Consequently, the combination of the NCF with the FBG enables to compensate this shift. Similarly, a hybrid fiber grating configuration combining a long period fiber grating (LPFG) and an FBG in series is utilized in [13]. The LPFG is used to monitor the SRI change while the FBG enables to compensate the temperature. There are also FBG-based sensors for multi-parameter sensing, as in [14], where temperature and SRI are measured with a point by point FBG; or [15], in which the same structure is employed for measuring these two variables and the liquid level. On the other hand, TFBGs are also utilized in hybrid configurations for measuring several parameters, as in [16], where a LPFG is employed for measuring the temperature while the TFBG enables to monitor the SRI, or in [17], in which a surface plasmon resonance (SPR) is combined with a TFBG for measuring the SRI while compensating the temperature.

Temperature compensation mechanisms are also applied to sensors manufactured on D-shaped fibers. In [18], a long-range surface plasmon resonance (LRSPR) sensor is used to measure the refractive index with temperature compensation. The LRSPR sensor has a dielectric buffer layer (DBL) made of fluorine-containing organic complexes of Terbium(III) and a Au thin film on the D-shaped region. The Terbium(III) complexes absorb light at around 350 nm and the absorption intensity is temperature dependent. This phenomenon enables temperature compensation. On the other hand, a SPR based on a D-shaped fiber is proposed in [19]. The sensor is based on the deposition of an Au film, half of which is coated with polydimethylsiloxane (PDMS). The first half (only Au) is used for SRI sensing, whilst the second one (with PDMS) for temperature sensing, compensating the temperature effect on the first half.

Regarding LMRs, temperature sensors have been developed with the purpose of measuring temperature, not compensating a temperature drift when measuring another variable. In [20], a soda-lime planar waveguide with a CuO thin film is presented. Similarly to the sensor in [19], the first part of the waveguide is used to measure the SRI while the second part is covered with PDMS and employed to measure the temperature, although no temperature compensation of the SRI measurement is done. Another example with a planar waveguide is described in [21], where a coverslip is deposited on both faces with a thin film. Here, two resonances are obtained, each one belonging to a different face of the coverslip; one is used to measure temperature with a PMDS coating and the other humidity thanks to an agarose coating.

Finally, it is also worth mentioning the existence of integrated photonic sensors for the measurement of the refractive index with temperature compensation, being their compact size their main advantage. In [22], an array of integrated slot-waveguide ring resonators with on chip temperature compensation is introduced. The temperature drift of the ring resonator in

Optics EXPRESS

which the refractive index of the liquid is being measured is compensated with the temperature measurement of another ring resonator in good thermal contact.

In this work, a titanium dioxide (TiO_2) thin film was deposited on the D-shaped region of an optical fiber to obtain a refractometer, and the temperature drift of the refractometer is compensated with a temperature sensor consisting of an FBG inscribed in the core of the D-shaped region, see Fig. 1. This is the first time that a thermo-refractometer of these characteristics has been developed based on LMRs and FBG and totally integrated in the fiber forming a unique sensor without any additional material covering the metallic oxide.

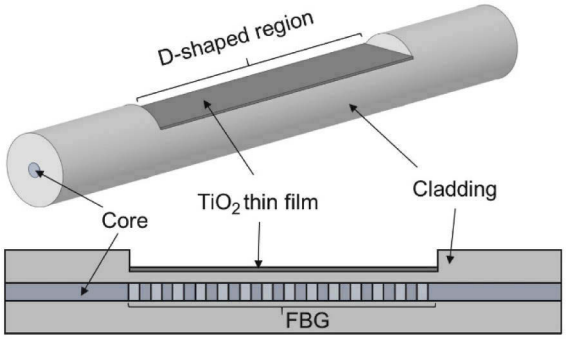

Fig. 1. Designed thermo-refractometer consisting of an FBG inscribed in the core and a TiO_2 nano-film covering the D-shaped region (top) and section view of the device (bottom).

2. Materials and methods

2.1. Materials and sensor fabrication

D-shaped fibers were purchased from Phoenix Photonics LTD and consist of standard single mode fibers (Corning SMF-28) with a cladding/core diameter of 125/8 μm and a polished length of 10 mm. These fibers are polished until obtaining an attenuation peak of 0.5 dB at 1550 nm in high refractive index oil (RI = 1.5).

Initially, fiber Bragg gratings (FBGs) with a period of 529.8 nm over a length of 3 mm are inscribed using phase mask method by a Coherent Xantos XS laser at 193 nm emission wavelength, 250 Hz repetition rate and 1.5 mJ/pulse in the core of the D-shaped region of the fiber, providing an FBG peak at around 1533 nm.

Afterwards, a thin film of 60 nm of TiO_2 is deposited onto the D-shaped zone using the atomic layer deposition (ALD) technique with the Savannah G2 ALD System from Veeco Inc. TiO_2 has been selected because this material provides a good SRI sensitivity (4122 nm/RIU for a D-shaped LMR based refractometer with the resonant wavelength at 1300 nm in [23]).This thickness was chosen in order to obtain a first order LMR_{TE} at a wavelength of around 1400 nm. This means that the FBG peak is far enough to guarantee that the resonance does not affect the intensity of the FBG.

2.2. Experimental setup

In the measuring setup, see Fig. 2, a multi-SLD light source (FJORD-X3-1330-1650, Pyroistech S.L.) is connected to input 1 of an optical circulator through an in-line polarizer and a polarization controller (Phoenix Photonics Ltd), which enables selecting the TE- or TM-polarized state of light [24]. One end of the D-shaped optical fiber is connected to output 2 of the circulator and the other end of the fiber is connected to an optical spectrum analyser (MS9740A from Anritsu) to monitor the power in transmission. Once the polarization state has been adjusted, the fiber is

Optics EXPRESS

fixed so the polarization state does not change. Output 3 of the optical circulator is connected to an interrogator (I-MON 512 USB from Ibsen Photonics A/S) that enables to monitor the FBG peak in reflection.

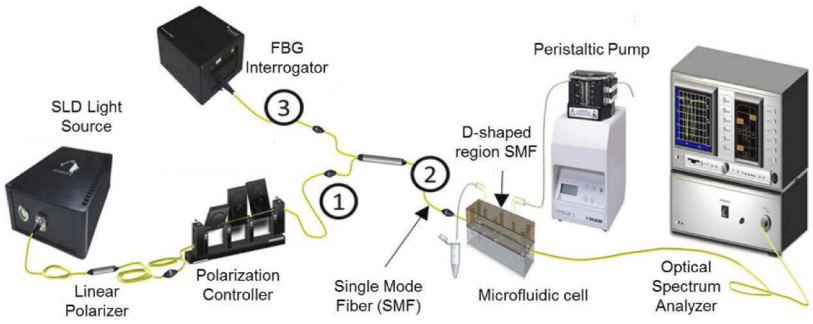

Fig. 2. Experimental setup scheme.

The D-shaped region is placed inside a microfluidic system that is thermo-stabilized by means of two Peltier cells, as in [25]. It consists of two equal-size pieces, the upper one is made of ULTEM and the lower one is made of stainless steel. A microfluidic channel is engraved on both bars with dimensions 1 mm × 1 mm × 50 mm (volume of 50 µL), with the D-shaped region fitting in this channel. A peristaltic pump allows to control the flow through the cell.

3. Results

Two assays were carried out with the setup shown in Fig. 2. In the first experiment, the device response was monitored with five different refractive indices, while the temperature was stabilized to 25°C. The LMR response is shown in Fig. 3 whilst the FBG response is shown in Fig. 4. The first refractive index corresponds to ultrapure water and the remaining four correspond to solutions of glucose in ultrapure water with values of 1.3324, 1.3367, 1.3407, 1.3445 and 1.3479 respectively, measured at 589.3 nm with refractometer Refracto30GS (Mettler Toledo Inc). The device was tested with these indices because the aim is to use it with liquids of refractive index close to that of water.

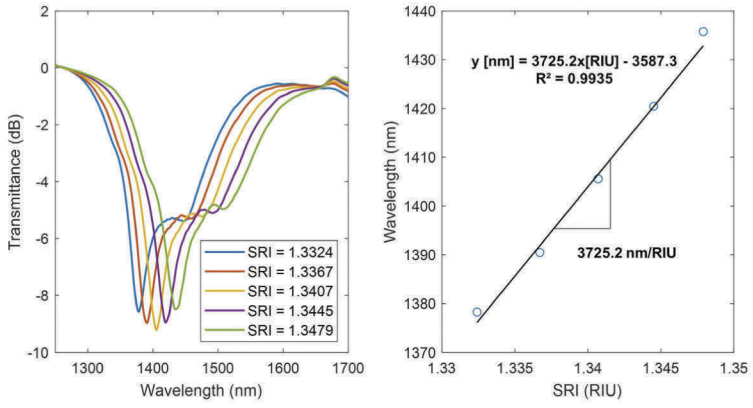

Fig. 3. Spectral response of the LMR when the D-shaped region is immersed in five different refractive index.

Optics EXPRESS

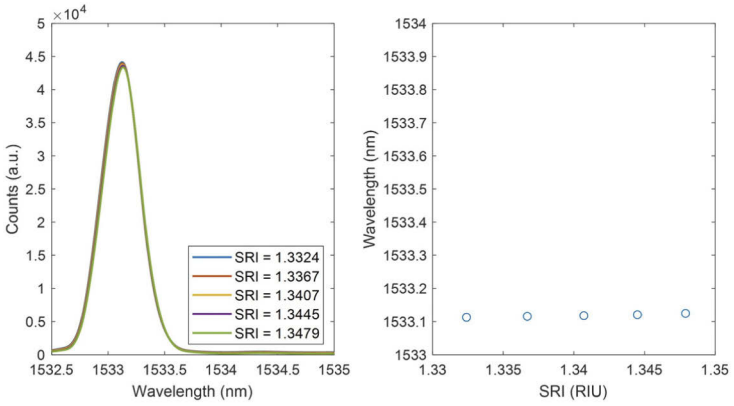

Fig. 4. Spectral response of the FBG when the D-shaped region is immersed in five different refractive index.

In Fig. 3 it can be observed that the resonance wavelength shifts linearly with a sensitivity of 3725.2 nm/RIU in the studied range. In Fig. 4, it can be seen that the FBG peak shift with refractive index is very small. In particular, the variation of the FBG peak in the studied SRI range was of only 12 pm, which corresponds to a sensitivity lower than 1 nm/RIU, which is negligible in comparison with the LMR sensitivity to the SRI. The FBG peak is slightly sensitive to the SRI as the cladding thickness between the core and the polished surface of the fiber is very thin (6.5 μm), as it happens in the case of FBGs inscribed in etched fibers [5].The choice of the axis limits in Fig. 4 is made to enable a direct comparison with Fig. 6. Before performing the second experiment, in which the temperature is varied, the system returns to the initial operating conditions (ultrapure water). It can be checked that the starting operation points of both experiments (LMR resonance located at 1378 nm and FBG peak at 1533.1 nm) are virtually the same, although there is sometimes a small hysteresis when returning to the initial operating conditions after a SRI variation and/or a temperature variation.

The second experiment consisted in varying the temperature from 25°C to 45°C in steps of 5°C while maintaining the D-shaped region of the fiber immersed in ultrapure water. The LMR response for this assay is presented in Fig. 5 while the FBG response is shown in Fig. 6. In this second experiment, the shape of the resonance is different compared to that observed in Fig. 3, because it is difficult to reproduce the very same polarization state in both experiments. Slight variations in the polarization state adjusted with the polarization controller lead to differences in the depth of the main resonance around 1380 - 1400 nm (slightly deeper in Fig. 5 compared with Fig. 3) and the residual lobe that appears at higher wavelengths (deeper in Fig. 5).

Regarding the results of the second experiment, in Fig. 5, the resonance wavelength shifts towards the blue when the temperature increases. The purpose of the plot on the right of Fig. 5 will be explained afterwards. In Fig. 6, the FBG peak shifts towards the red when the temperature increases, with a sensitivity of 32.6 pm/°C and following a linear response. The expected temperature sensitivity for an FBG at around 1550 nm is approximately 13.7 pm/°C [11]. In the case under study, the FBG is inscribed in the core of a fiber that is glued to the upper half of the microfluidic cell. Therefore, the dilatation of the microfluidic cell with temperature affects the temperature sensitivity.

The results from the previous experiments can be employed to obtain a sensitivity matrix that correlates the variation in the SRI and temperature (ΔSRI and ΔT respectively) between two operation points with the wavelength shifts of the LMR and the FBG ($\Delta\lambda_{LMR}$ and $\Delta\lambda_{FBG}$

Optics EXPRESS

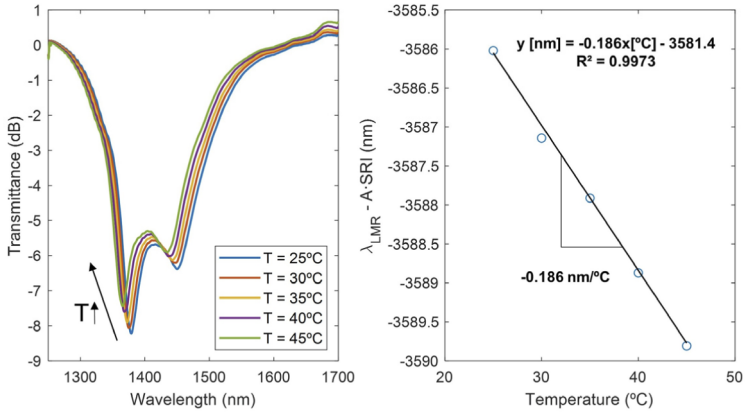

Fig. 5. Spectral response of the LMR when the temperature is varied (left) and calculation of coefficient B (right).

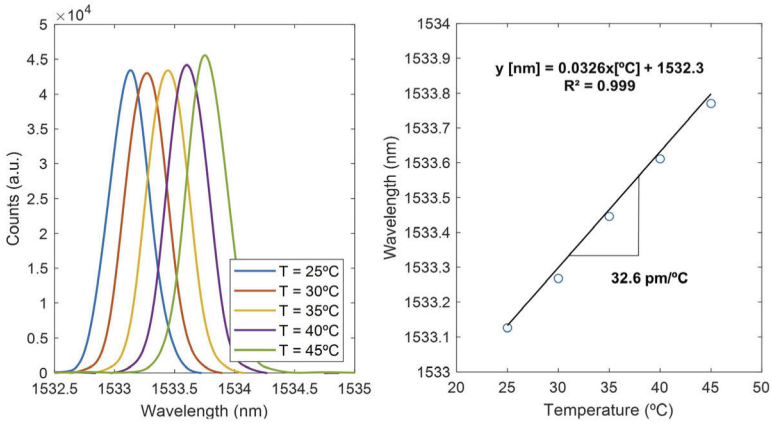

Fig. 6. Spectral response of the FBG when the temperature is varied.

respectively), as it is shown in Eq. (2).

$$\begin{pmatrix} \Delta\lambda_{LMR} \\ \Delta\lambda_{FBG} \end{pmatrix} = \begin{bmatrix} A & B \\ C & D \end{bmatrix} \begin{pmatrix} \Delta SRI \\ \Delta T \end{pmatrix} \tag{2}$$

In the first experiment $\Delta T = 0$, so $\Delta\lambda_{LMR} = A \cdot \Delta SRI$ and from Fig. 3, $A = 3725.2$ nm/RIU. The FBG sensitivity to the SRI is negligible in comparison to the LMR sensitivity, as it can be checked in Fig. 4, thus it can be considered that $C = 0$.

In the second experiment, both ΔSRI and ΔT are different from 0. The SRI changes because the refractive index of a liquid varies with temperature. However, as $C = 0$, $\Delta\lambda_{FBG} = D \cdot \Delta T$, and from Fig. 6, $D = 32.6$ pm/°C. Finally, B can be calculated from Eq. (2) as:

$$B = \frac{\Delta\lambda_{LMR} - A \cdot \Delta SRI}{\Delta T} = \frac{\Delta(\lambda_{LMR} - A \cdot SRI)}{\Delta T} \tag{3}$$

Therefore, if $\lambda_{LMR} - A \cdot SRI$ is plotted vs the temperature, B is the slope of the linear response that is obtained, as it is shown on the right of Fig. 5, with B = -0.186 nm/°C. The values of the SRI of water for the different temperatures have been obtained from [26].

Optics EXPRESS

The calibration to obtain these coefficients should be repeated each time a new fiber is employed by simply following the previous steps, which could be performed automatically if necessary.

If both sides of Eq. (2) are multiplied by the inverse of the sensitivity matrix, the unknown ΔSRI and ΔT for certain values of $\Delta\lambda_{LMR}$ and $\Delta\lambda_{FBG}$ can be obtained, as it is shown in Eq. (4). The values that correspond to this case are substituted in Eq. (5).

$$\begin{pmatrix} \Delta SRI \\ \Delta T \end{pmatrix} = \begin{bmatrix} A & B \\ C & D \end{bmatrix}^{-1} \begin{pmatrix} \Delta\lambda_{LMR} \\ \Delta\lambda_{FBG} \end{pmatrix} (4) \tag{4}$$

$$\begin{pmatrix} \Delta SRI \\ \Delta T \end{pmatrix} = \begin{bmatrix} 2.684 \cdot 10^{-4} & 1.532 \cdot 10^{-3} \\ 0 & 30.675 \end{bmatrix}^{-1} \begin{pmatrix} \Delta\lambda_{LMR} \\ \Delta\lambda_{FBG} \end{pmatrix} (5) \tag{5}$$

Once ΔSRI and ΔT are obtained, the temperature of the final operation point and the value of the SRI at that temperature can be calculated if these values are known at the initial operation point. Note that, as opposed to other sensors, the SRI value is not provided at the initial reference temperature, but at the temperature that is being measured simultaneously.

With this calibration, the intrinsic drift with temperature of the device is compensated, so the device can be employed to measure the temperature and the refractive index not only of ultrapure water, the liquid used in the calibration, but also of other liquids. In order to demonstrate the importance of this calibration, the results of supposing $B = 0$, that is, not compensating the effect of the temperature over the device operation, are shown in Table 1 for the results of the second experiment.

Table 1. Error committed when supposing B = 0.

T (°C)	SRI (RIU)	$\Delta\lambda_{LMR}$ (nm)	ΔSRI (RIU) ($B = 0$)	SRI (RIU) ($B = 0$)	Error (%)
25	1.3328	0	0	1.3328	0
30	1.3323	-3.10	-8.31E-04	1.3320	-0.02
35	1.3316	-6.36	-1.71E-03	1.3311	-0.04
40	1.3310	-9.85	-2.65E-03	1.3302	-0.06
45	1.3302	-13.73	-3.69E-03	1.3291	-0.08

The first three columns in Table 1 correspond to the temperature (°C), the real SRI (RIU) calculated from [26] and $\Delta\lambda_{LMR}$ (nm) respectively. The fourth column corresponds to ΔSRI (RIU) assuming $B = 0$ (wrong calculation). The fifth column corresponds to the wrong SRI (RIU) derived from the wrong ΔSRI and the last column to the relative error in %. It can be deduced from this table that the effect of temperature on the device operation cannot be ignored for applications where a precise measurement of the SRI is required, such as gas sensing or biosensing applications. Although the error might seem negligible in percentage, it becomes more relevant if it is taken into account that it can affect the fourth and third decimals of the SRI.

For the sake of comparison, a table with the main characteristics of this device and the works described in the introduction, where both the SRI and the temperature are measured, is included (see Table 2). It can be observed that the SRI sensitivity of the developed device is high when compared with sensors included in Table 2 (only surpassed by [18]), specially taking into account that most devices are tested with higher values of the SRI. However, it must be considered that there are refractometers similar to the one developed, based on a D-shape structure, with much higher sensitivities, such as the ones described in Refs. [6] (5855 nm/RIU for an LMR based on ITO), [27] (14,501 nm/RIU for an LMR based on SnO_2) or [28] (22,779 nm/RIU for an SPR obtained with Au deposited on a polymer fiber); although these devices do not

Optics EXPRESS

measure the temperature. It would be interesting to reach these sensitivities while maintaining the temperature measuring capability. Regarding the temperature sensitivity, its value is good compared with other sensors that employ FBGs [14,15] but low in the case of the sensors that combine resonances with the use of PDMS ([19,20].

Table 2. Comparison with other works where both the SRI and the temperature are measured.

SRI sensing mechanism	SRI sensitivity (nm/RIU)	SRI range (RIU)	Temperature measuring mechanism	Temperature sensitivity	Temperature range (°C)	Ref.
FBG	1.284 - 12.77	1.3333 - 1.3800	FBG	9.39 - 10.07 pm/°C	25 - 65.5	[14]
FBG	535.14	1.33 - 1.454	FBG	10.06 pm/°C	20.3 - 99.5	[15]
TFBG	606.82	1.3761 - 1.4327	LPFG	268.79 pm/°C	-30 - 70	[16]
TFBG-SPR	571.5	1.3325–1.3375	TFBG-SPR	6.3pm/°C	23 - 59	[17]
LRSPR	4111.67	1.3317 - 1.3365	Terbium(III) absorption	0.05 dB/°C	15 - 50	[18]
SPR	2260.1	1.333 - 1.390	SPR + PDMS	-2.41 nm/°C	20 - 60	[19]
LMR	1460	1.3328 - 1.37	LMR + PDMS	-1.75 nm/°C	20 - 40	[20]
Slot waveguide ring resonator	240	(not provided)	Slot waveguide ring resonator	16.6 pm/°C	23 - 33	[22]
LMR	3725.2	1.3324–1.3479	FBG	32.6 pm/°C	25 - 45	This work

4. Conclusions

The proposed device has been successfully validated to obtain a refractometer where the temperature influence over the device has been eliminated while the temperature value is measured simultaneously at the same point. In particular, the SRI has been measured in the range from 1.3324 to 1.3479 with a sensitivity of 3725.2 nm/RIU while the temperature varied from 25°C to 45°C.

It must also be remarked that this is the first time that a fully integrated thermo-refractometer consisting of a thin film deposited on a D-shaped optical fiber and an FBG inscribed in its core has been presented. This device could be improved by using an exclusively reflection setup instead of requiring both reflection and transmission interrogation. This can be achieved with an Ag mirror on the tip of the fiber and monitoring the LMR in reflection as in [29]. Furthermore, the proposed device could be miniaturized in a 2 mm long device or even less, as it has been demonstrated that a 2 mm long D-shaped fiber with a nanocoating can generate LMRs for sensing purposes [29] while femtosecond laser technique permits to obtain very short FBGs, on the order of 100 μm [30]. This has special interest in the development of small size probes or the employment of multiple sensors is a small area.

These results also open the door for applications where the LMR shift permits to precisely monitor refractometric changes associated to a single parameter or analyte while the FBG is used to measure a different parameter or analyte, therefore obtaining a totally integrated dual sensor. This concept could be extrapolated to other grating based structures such as TFBGs or LPFGs.

Funding. Ministerio de Ciencia, Innovación y Universidades (FPU18/03087, PID2019-106231RB-I00 TEC); Universidade Tecnológica Federal do Paraná; Conselho Nacional de Desenvolvimento Científico e Tecnológico.

Disclosures. The authors declare no conflict of interest.

Data availability. Data underlying the results presented in this paper are not publicly available at this time but may be obtained from the authors upon reasonable request.

Optics EXPRESS

References

1. D. Beysens and P. Calmettes, "Temperature dependence of the refractive indices of liquids: Deviation from the Lorentz–Lorenz formula," J. Chem. Phys. **66**(2), 766–771 (1977).
2. P. Roriz, S. Silva, O. Frazão, and S. Novais, "Optical Fiber Temperature Sensors and Their Biomedical Applications," Sensors **20**(7), 2113 (2020).
3. I. Del Villar, F. J. Arregui, C. R. Zamarreño, J. M. Corres, C. Bariain, J. Goicoechea, C. Elosua, M. Hernaez, P. J. Rivero, A. B. Socorro, A. Urrutia, P. Sanchez, P. Zubiate, D. Lopez, N. De Acha, J. Ascorbe, and I. R. Matias, "Optical sensors based on lossy-mode resonances," Sensors and Actuators B: Chemical **240**, 174–185 (2017).
4. C. Ruiz Zamarreño, P. Zubiate, M. Sagües, I. R. Matias, and F. J. Arregui, "Experimental demonstration of lossy mode resonance generation for transverse-magnetic and transverse-electric polarizations," Opt. Lett. **38**(14), 2481 (2013).
5. A. Urrutia, I. Del Villar, P. Zubiate, and C. R. Zamarreño, "A Comprehensive Review of Optical Fiber Refractometers: Toward a Standard Comparative Criterion," Laser Photon. Rev. **13**(11), 1900094 (2019).
6. P. Zubiate, C. R. Zamarreño, I. Del Villar, I. R. Matias, and F. J. Arregui, "High sensitive refractometers based on lossy mode resonances (LMRs) supported by ITO coated D-shaped optical fibers," Opt. Express **23**(6), 8045 (2015).
7. A. Ozcariz, C. R. Zamarreño, P. Zubiate, and F. J. Arregui, "Is there a frontier in sensitivity with Lossy mode resonance (LMR) based refractometers?" Sci. Rep. **7**(1), 10280–7 (2017).
8. A. Ozcariz Celaya, "Materials for the fabrication of optical fiber refractometers based on lossy mode resonance," Sensors **20**(7), 1972 (2020).
9. C. R. Zamarreño, F. J. Arregui, I. Del Villar, I. R. Matias, and P. Zubiate, "Optimization in nanocoated D-shaped optical fiber sensors," Opt. Express **25**(10), 10743–10756 (2017).
10. K. O. Hill and G. Meltz, "Fiber Bragg grating technology fundamentals and overview," J. Light. Technol. **15**(8), 1263–1276 (1997).
11. A. Othonos, "Fiber Bragg gratings," Rev. Sci. Instrum. **68**(12), 4309–4341 (1997).
12. C. Li, T. Ning, C. Zhang, J. Li, X. Wen, L. Pei, X. Gao, and H. Lin, "Liquid level measurement based on a no-core fiber with temperature compensation using a fiber Bragg grating," Sensors Actuators," A Phys. **451**, 49–62 (2016).
13. L. Alwis, T. Sun, and K. T. V. Grattan, "Optical Fibre Refractive Index Sensor in a Hybrid Fibre Grating Configuration," Procedia Eng. **120**, 11–14 (2015).
14. C. Zhu, D. Alla, J. Huang, J. Huang, and J. Huang, "High-temperature stable FBGs fabricated by a point-by-point femtosecond laser inscription for multi-parameter sensing," OSA Contin. **4**(2), 355–363 (2021).
15. K. Yang, B. Liu, C. Liao, Y. Wang, Z. Cai, J. Tang, Y. Yang, and Y. Wang, "Highly Localized Point-by-Point Fiber Bragg Grating for Multi-Parameter Measurement," J. Light. Technol. **39**(20), 6686–6690 (2021).
16. X. Fan, J. Jiang, X. Zhang, K. Liu, S. Wang, and T. Liu, "Simultaneous measurement of refractive index and temperature using a hybrid-grating sensor," Appl. Phys. Express **12**(11), 116501 (2019).
17. L.-Y. Shao, Y. Shevchenko, and J. Albert, "Intrinsic temperature sensitivity of tilted fiber Bragg grating based surface plasmon resonance sensors," Opt. Express **18**(11), 11464 (2010).
18. Q. Wang, J. Y. Jing, X. Z. Wang, L. Y. Niu, and W. M. Zhao, "A D-Shaped Fiber Long-Range Surface Plasmon Resonance Sensor with High Q-Factor and Temperature Self-Compensation," IEEE Trans. Instrum. Meas. **69**(5), 2218–2224 (2020).
19. L. Liu, Z. Liu, Y. Zhang, and S. Liu, "Side-Polished D-Type Fiber SPR Sensor for RI Sensing with Temperature Compensation," IEEE Sens. J. **21**(15), 16621–16628 (2021).
20. O. Fuentes, J. M. Corres, I. Dominguez, I. Del Villar, and I. R. Matias, "Lossy mode resonances generated in planar configuration for two-parameter sensing," *IEEE Sens. J.* 1 (2021).
21. I. Dominguez, I. Del Villar, O. Fuentes, J. M. Corres, and I. R. Matias, "Dually nanocoated planar waveguides towards multi-parameter sensing," Sci. Rep. **11**(1), 3669 (2021).
22. A. Kaźmierczak, C. F. Carlborg, C. A. Barrios, F. Dortu, G. Stemme, H. Sohlström, K. B. Gylfason, L. Vivien, and W. van der Wijngaart, "On-chip temperature compensation in an integrated slot-waveguide ring resonator refractive index sensor array," Opt. Express **18**(4), 3226–3237 (2010).
23. C. L. Tien, H. Y. Lin, and S. H. Su, "High Sensitivity Refractive Index Sensor by D-Shaped Fibers and Titanium Dioxide Nanofilm," Adv. Condens. Matter Phys. **2018**, 1–6 (2018).
24. F. Chiavaioli, P. Zubiate, I. Del Villar, C. R. ZamarrenÌo, A. Giannetti, S. Tombelli, C. Trono, F. J. Arregui, I. R. Matias, and F. Baldini, "Femtomolar Detection by Nanocoated Fiber Label-Free Biosensors," ACS Sens. **3**(5), 936–943 (2018).
25. P. Zubiate, A. Urrutia, C. R. Zamarreño, J. Egea-Urra, J. Fernández-Irigoyen, A. Giannetti, F. Baldini, S. Díaz, I. R. Matias, F. J. Arregui, E. Santamaría, F. Chiavaioli, and I. Del Villar, "Fiber-based early diagnosis of venous thromboembolic disease by label-free D-dimer detection," ACS Sens. **2**, 100026 (2019).
26. A. N. Bashkatov and E. A. Genina, "Water refractive index in dependence on temperature and wavelength: a simple approximation," in *Proceedings Volume 5068, Saratov Fall Meeting 2002: Optical Technologies in Biophysics and Medicine IV* (SPIE, 2003), 5068, pp. 393–395.
27. F. J. Arregui, I. Del Villar, C. R. Zamarreño, P. Zubiate, and I. R. Matias, "Giant sensitivity of optical fiber sensors by means of lossy mode resonance," Sensors Actuators, B Chem. **232**, 660–665 (2016).

Optics EXPRESS

28. S. Cao, Y. Shao, Y. Wang, L. Zhang, Y. Huang, F. Zhang, C. Liao, Y. Wang, K. V. Sreekanth, Y. Alapan, M. ElKabbash, E. Ilker, M. Hinczewski, U. A. Gurkan, A. De Luca, and G. Strangi, "Highly sensitive surface plasmon resonance biosensor based on a low-index polymer optical fiber," Opt. Express **26**(4), 3988–3994 (2018).
29. O. Fuentes, P. Vaiano, I. del Villar, G. Quero, J. Corres, M. Consales, I. Matías, and A. Cusano, "Improving the width of lossy mode resonances in a reflection configuration D-shaped fiber by nanocoating laser ablation," Opt. Lett. **45**(17), 4738 (2020).
30. C. Hnatovsky, D. Grobnic, and S. J. Mihailov, "Through-the-coating femtosecond laser inscription of very short fiber Bragg gratings for acoustic and high temperature sensing applications," Opt. Express **25**(21), 25435–25446 (2017).